Role of Thermal Heating on the Voltage Induced Insulator-Metal Transition in VO_2

A. Zimmers,[1,*] L. Aigouy,[1,†] M. Mortier,[2] A. Sharoni,[3] Siming Wang,[4,5,6] K. G. West,[4,5] J. G. Ramirez,[4,5] and Ivan K. Schuller[4,5,6]

[1]*Laboratoire de Physique et d'Etude des Matériaux, UMR 8213, ESPCI-ParisTech-CNRS-UPMC, 10 rue Vauquelin, 75231 Paris, France*

[2]*Laboratoire de Chimie de la Matière Condensée de Paris, UMR 7574, Chimie-ParisTech–CNRS, 11 rue Curie, 75231 Paris, France*

[3]*Department of Physics and Institute of Nanotechnology, Bar Ilan University, Ramat Gan 52900, Israel*

[4]*Department of Physics, University of California San Diego, La Jolla, California 92093, USA*

[5]*Center for Advanced Nanoscience, University of California San Diego, La Jolla, California 92093, USA*

[6]*Materials Science and Engineering Program, University of California San Diego, La Jolla, California 92093, USA*

(Received 23 April 2012; revised manuscript received 6 September 2012; published 29 January 2013)

We show that the main mechanism for the dc voltage or dc current induced insulator-metal transition in vanadium dioxide VO_2 is due to local Joule heating and not a purely electronic effect. This ''tour de force'' experiment was accomplished by using the fluorescence spectra of rare-earth doped micron sized particles as local temperature sensors. As the insulator-metal transition is induced by a dc voltage or dc current, the local temperature reaches the transition temperature indicating that Joule heating plays a predominant role. This has critical implications for the understanding of the dc voltage or dc current induced insulator-metal transition and has a direct impact on applications which use dc voltage or dc current to externally drive the transition.

DOI: 10.1103/PhysRevLett.110.056601 PACS numbers: 72.70.+m, 71.30.+h, 72.20.−i

The insulator-metal transition (IMT) in oxides is an intensely investigated phenomenon which has received considerable attention from the basic research community and has potential as the basis for revolutionary applications in electronics, smart optics, energy technologies, data storage, and neuromorphic circuits [1] (and references therein). In this class of materials, the electrical resistivity can change, by as much as 5 orders of magnitude, at a material-dependent transition temperature. The origin of this hysteretic, first order phase transition is still debated and the exact nature of the phase transition is not understood. Recently, the possibility of inducing the IMT phase transition with a dc voltage or current has produced much excitement because it opens the possibility of inducing new functionalities into materials which can be controlled by external means (other than temperature) [2,3]. In several metal oxides which have thermally induced IMT (such as VO_2, Fe_3O_4), the dc voltage induced switching mechanism remains controversial as it may originate from an electronic order breakdown [4–9] or from local heating [10,11]. While it was shown that there is no global temperature change, establishing this at the local scale has not been done and is very challenging. In this Letter, we show in the prototypical VO_2 [12,13] by direct, local, quantitative, thermal measurements that local Joule heating plays a predominant role in the dc voltage (or dc current) induced IMT. These observations have a major impact on theories of the dc voltage induced IMT and will seriously impact applications which rely on IMT driven by external means other than temperature. Note that our data address exclusively the dc voltage induced IMT and do not shed light on the mechanism of the thermally induced IMT.

Vanadium dioxide (130 nm thick) thin films were prepared by reactive rf magnetron sputtering of a 1.5″ V_2O_3 target (>99.7%, ACI Alloys, Inc.) on an *r*-cut sapphire substrate. A mixture of ultrahigh purity argon and ultrahigh purity oxygen was used for sputtering. The total pressure during deposition was 4 mTorr, and the oxygen partial pressure was optimized to 0.1 mTorr (2.5% of the total pressure). The substrate temperature during deposition was 600 °C while the rf magnetron power was kept at 100 W. 50 μm width VO_2 ribbons were patterned and gold electrodes were deposited on top of the film to make microchannels [see Fig. 2(a)]. Two channels of 10 and 20 μm width were used for this study.

Four-probe $R(T)$ measurements were performed in a cryostat (PPMS, Quantum Design). $R(T)$ measurements [Fig. 1(a)] show a transition temperature of 339 K (66 °C) as T increases [14–16], a resistance drop of more than 4 orders of magnitude indicative of high quality thin film, a transition width of 5 °C, and a hysteresis of 5 °C. Two-probe $R(T)$ and four-probe $R(T)$ measurements superimpose within a few percent meaning that contact resistance is very low compared to the VO_2 film resistance in the insulating state.

Beyond a critical voltage applied across these channels ($V_{\text{threshold}}$), a single IMT switching occurs as shown in Fig. 1(b). $V_{\text{threshold}}$ varies from 15 to 52 V depending on the channel size and set temperature, which corresponds

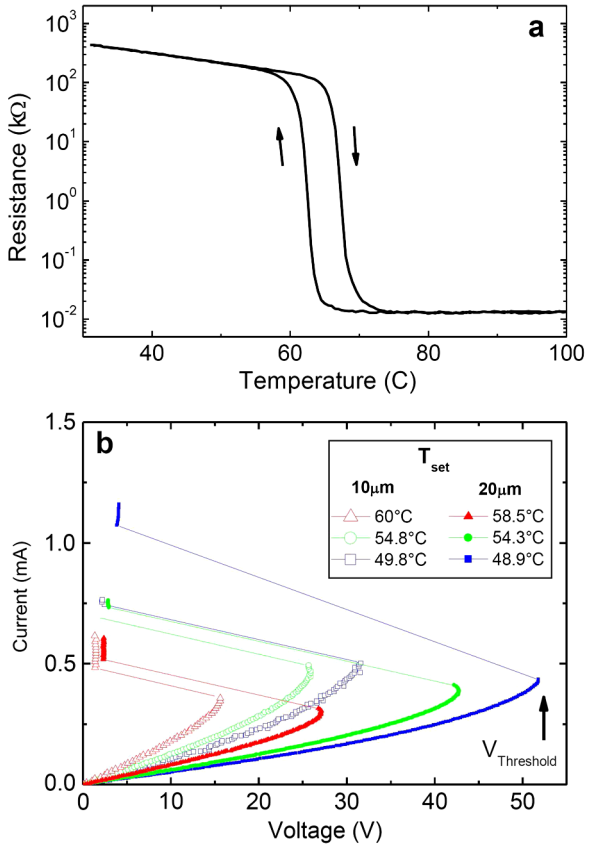

FIG. 1 (color online). (a) Four-probe measurement of thermally induced IMT. (b) Two-probe nonequilibrium transport measurements of the 10 μm (open symbols) and 20 μm channels for various set temperatures T_{set} set by the Peltier heater under the sample. The schematic circuit used is presented in Fig. 2(b). The dc voltage applied across the channel is obtained by subtracting the dc voltage drop across both resistances placed in series to the generator dc applied voltage. The dc current in the circuit is measured by acquiring the dc voltage drop across a 55 kΩ resistance placed in series. Above $V_{threshold}$ [identified as an example by a vertical arrow on one of the curves in (b)], in the low resistance state of VO_2, the dc current flowing in the circuit is limited by the 123 and 55 kΩ resistances placed in series.

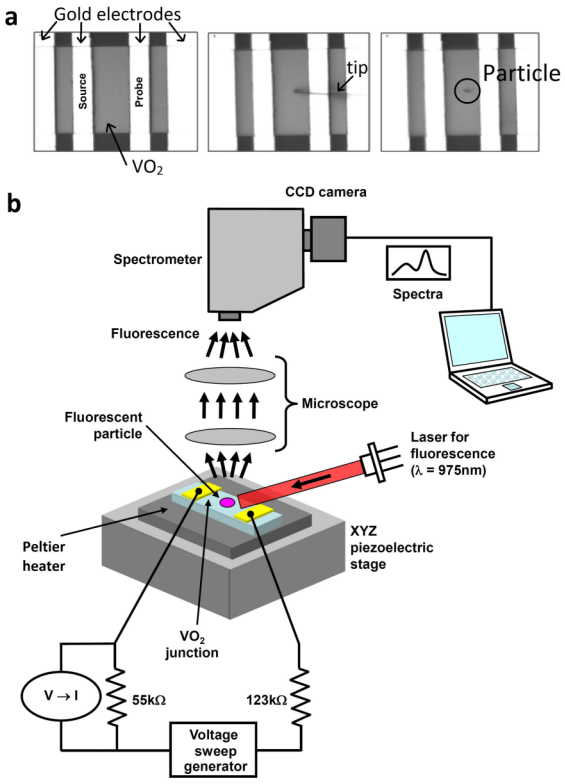

FIG. 2 (color online). (a) 20 μm channel before, during, and after positioning the micron-wide rare-earth fluorescent particle (from left to right). Right-hand image: The four gold electrodes identified were used in the four-probe measurements ($I+$, $V+$, $V-$, $I-$ from left to right); the indicated "source" and "probe" gold electrodes were used in the two-probe measurements. (b) Description of the experimental optical and electrical setup.

to an electric field across the channel, $E_{threshold} = V_{threshold}$/channel size, ranging from 1.5 to 2.6 10^6 V/m (as reported previously [17]).

The local temperature measurements are performed using a fluorescent particle inside the channel. An optical image of the 20 μm channel is shown in Fig. 2(a). To place the particle in the channel, it was first attached to the end of a sharp tungsten tip [18] and then positioned in the microchannel using a homemade nanomanipulator system. Figure 2(a) shows the micrometer channel before, during, and after placing the particle (from left to right). Note that the size of the particle (~ 1 μm) determines the size of the region where temperature is probed. The fluorescent material is a fluoride glass codoped with erbium and ytterbium ions [19]. When excited in the near-infrared spectral region ($\lambda = 975$ nm), the material emits visible light after absorption of two photons (up-conversion process). The two emission lines, at $\lambda = 520$ nm and $\lambda = 550$ nm, arise from energy levels which are in thermal equilibrium. Their relative area (A_{520} and A_{550}, respectively) allows the determination of the temperature (in kelvin) from the previously reported relation [19–21]:

$$\frac{A_{520}}{A_{550}} = Be^{-D/T}. \quad (1)$$

An accurate temperature measurement requires precise determination of the B and D parameters for the specific particle used in the experiment. The experimental setup for the calibration and for the temperature measurements across the VO_2 channel is shown in Fig. 2(b). We first measured the spectra and deduced the peak area ratio of the particle on the VO_2 channel while heating it to fixed temperatures (T_{set}) using a Peltier heater under the sample. Simultaneously, we measured (two-probe) the channel resistances which gave two absolute calibration points: room temperature, 27 °C (Peltier heater off), and the IMT, 66 °C (sharp transition temperature determined

previously by PPMS). With these, $B = 7.25 \pm 0.3$ and $D = 1103 \pm 30$ K are in good agreement with literature values [19–21].

Using this calibration (shown in Fig. 3), we then performed the nonequilibrium $I(V)$ measurements starting at T_{set}: 60 °C, 54.8 °C, and 49.8 °C for the 10 μm and 58.8 °C, 54.3 °C, and 48.9 °C for the 20 μm channel. The nonequilibrium optical and $I(V)$ sweeps took typically 1 min to obtain. The local temperatures of the channels are plotted as a function of channel dc voltages in Fig. 4 and constitute the main findings of this Letter. As dc voltage increases through the channel, the dc current brings it to the thermally induced IMT region independently from the channel sizes or the set temperatures (the lowest starting temperature T_{set} was 17 °C below the thermally induced IMT). This shows that within these parameters, i.e., placing the VO_2 at T_{set} up to 17 °C under the thermally induced IMT with a ± 1 °C accuracy, the dc nonlinear switching in VO_2 can be explained by Joule heating. Note our results are for dc driven switching only and not for ultrafast charge injection [13] where the switching mechanism could still be due to electronic breakdown. Measuring the heating effect on these time scales currently remains impossible.

The heating can be modeled assuming Ohmic dissipation [22,23] using $T_{model} = T_{set} + \alpha IV$. We find $\alpha_{10\mu m} = 750 \pm 5$ °C/W for all 10 μm measurements and $\alpha_{20\mu m} = 600 \pm 10$ °C/W for all the 20 μm curves [one modeled heating curve is plotted for each channel in Figs. 4(a) and 4(c)]. Estimating the coefficient α remains a challenging task since it depends on parameters such as channel surface size and the heat sink into the gold leads and sapphire substrate. This could be approached for our specific geometries using COMSOL Multiphysics® simulation as done previously [5], but it is beyond the scope of this Letter.

As a consistency check, we have also replotted the same $R(T)$ in two different ways: (i) R measured while heating with the Peltier heater and T the temperature of the particle found in Fig. 4 [denoted as "Equilibrium $R(T)$" in Figs. 4(b) and 4(d)], (ii) R measured during the dc voltage sweeps (0 to 60 V) and T the temperature of the particle measured simultaneously [denoted as "Nonequilibrium $R(T)$" in Figs. 4(b) and 4(d)]. Both $R(T)$ curves superimpose on each other providing additional support for the importance of Joule heating. Note that for all curves presented in Fig. 4, the temperatures were measured using the peak area ratios of the fluorescent particle. This is essential in order to obtain consistent measurements. To check these

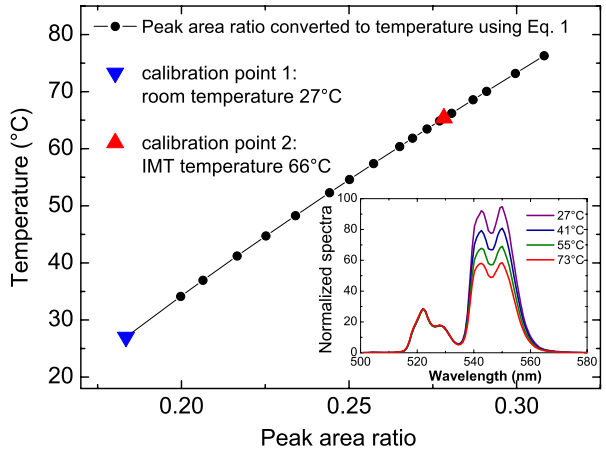

FIG. 3 (color online). Equivalence between fluorescent temperature and peak area ratio using Eq. (1) and both calibration points (room temperature 27 °C and thermally induced IMT 66 °C, error bars of these points are ±0.5 °C, which are smaller than the symbols used). Inset: Fluorescent 520 and 550 nm lines (normalized to equalize all 520 nm peak heights for clarity) as a function of set temperature T_{set} (only 4 spectra shown out of 18 for clarity) set by a Peltier heater under the sample.

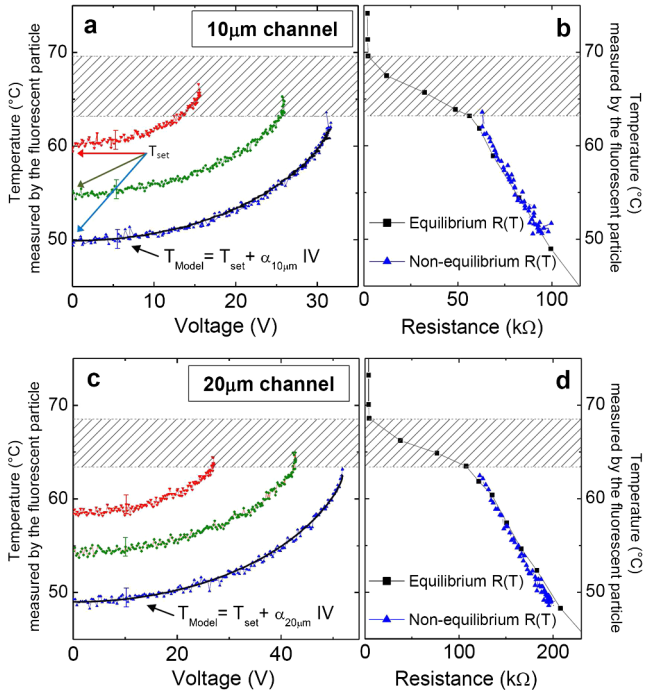

FIG. 4 (color online). Local temperature versus dc voltage [(a), (c)] and local temperature versus resistance [(b), (d)] for the 10 and 20 μm channels. Starting from T_{set}, the temperature rise due to Joule heating brings the VO_2 sample above the onset of the thermally induced IMT, i.e., inside the dashed regions (the thermal induced transition region). All curves are measured up to the dc voltage induced IMT. For local temperature after the switching at higher dc voltages, see discussion in the text and Fig. 5 for the data. Note that the power used by the Peltier device to heat the sample holder to T_{set} was maintained constant during each dc voltage sweep. Panels (b) and (d) also show the equilibrium $R(T)$ and nonequilibrium $R(T)$ data as explained in the main text. Panels (a) and (c) also show the Ohmic Joule heating model [22,23] $T_{model} = T_{set} + \alpha IV$ fitting the measured temperature rise.

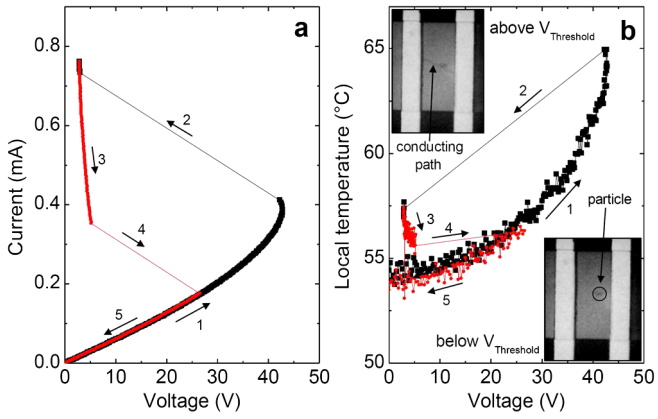

FIG. 5 (color online). dc switching hysteresis loops (paths 1–5) of transport (a) and thermal heating (b) of the 20 μm channel as a function of dc voltage (applied across the channel). Color code: Black as generator dc voltage rises and gray (red) as it goes down. (b) Inserted images of the channel above and below (top and bottom) $V_{\text{threshold}}$. The fluorescent particle and the conducting path are indicated for clarity. As dc voltage is applied (path 1) temperature rises from T_{set} (54.3 °C) to 65 °C [as already presented or discussed previously in Figs. 4(a) and 4(c)]. After the dc switching (path 2), the temperature drops by a few degrees to 58 °C. A conducting path is created (see narrow horizontal dark line in top image of (b)]. As the dc voltage generator reaches its maximum and starts ramping down (path 3), inverse dc switching occurs (path 4) from metallic back to insulating (the channel aspect transfers back to the lower image of the channel without conducting path). The transport falls back to the initial level, as does the temperature of the channel (path 5).

findings further we have also studied the channel homogeneity below and above $V_{\text{threshold}}$.

Below the dc voltage induced IMT, i.e., below $V_{\text{threshold}}$, we placed the fluorescent particle at various locations in the channel using the nanomanipulator. Within 0.5 °C we found no difference in heating below the dc voltage induced IMT.

Above the dc voltage induced IMT, i.e., above $V_{\text{threshold}}$, using an optical microscope, a very narrow conducting path can be observed after the IMT dc switching as reported previously [4,24] [see top image in Fig. 5(b)]. The path has been identified as conducting since it is in the same color as the sample heated to a fully metallic state using the Peltier heater under the thin film. The temperature of the particle after switching drops from 65 °C to 58 °C, thus suggesting that the fluorescent particle was not on the conducting path in this case [yet very close, as seen in the upper image of Fig. 5(b)] [25]. This temperature drop is most probably due to the lowering of the local dc current density in the VO_2 channel below the particle. Indeed, we expect the dc current density distribution above and below $V_{\text{threshold}}$ to change drastically; i.e., in the *metallic* state the dc current passes primarily through the conducting path, whereas in the *insulating* state it is more homogeneous.

Finally, with decreasing dc voltage across the channel, the reverse metal to insulator dc switching occurs as seen in the $I(V)$ curve, bringing back the temperature of the channel on the same slope as before. Cycling many times showed the same results; no aging effects were observed.

In conclusion, we showed using local, quantitative temperature measurements that Joule heating plays a major role in the dc voltage or dc current induced metal insulator transition in VO_2. With the application of a dc voltage or dc current, the heating before the transition is homogeneous across micron sized VO_2 channels, and as the transition is induced, local heating plays an essential role. These observations have important implications for fundamental understanding of the dc voltage induced IMT and affect in an essential way possible applications based on dc voltage or dc current induced transitions.

A. Z. acknowledges support from ANR Grant No. 09-BLAN-0388-01. Work at UCSD was supported by AFOSR Grant No. FA9550-12-1-0381.

*alexandre.zimmers@espci.fr
†lionel.aigouy@espci.fr

[1] Z. Yang, C. Ko, and S. Ramanathan, Annu. Rev. Mater. Res. **41**, 337 (2011).
[2] L. Chua, IEEE Trans. Circuit Theory **18**, 507 (1971).
[3] D. B. Strukov, G. S. Snider, D. R. Stewart, and R. S. Williams, Nature (London) **453**, 80 (2008).
[4] C. Berglund, IEEE Trans. Electron Devices **16**, 432 (1969).
[5] G. Gopalakrishnan, D. Ruzmetov, and S. Ramanathan, J. Mater. Sci. **44**, 5345 (2009).
[6] B. Wu, A. Zimmers, H. Aubin, R. Ghosh, Y. Liu, and R. Lopez, Phys. Rev. B **84**, 241410(R) (2011).
[7] S. Lee, A. Fursina, J. T. Mayo, C. T. Yavuz, V. L. Colvin, R. G. S. Sofin, I. V. Shvets, and D. Natelson, Nat. Mater. **7**, 130 (2007).
[8] T. Oka, R. Arita, and H. Aoki, Phys. Rev. Lett. **91**, 066406 (2003).
[9] T. Oka and H. Aoki, Phys. Rev. B **81**, 033103 (2010).
[10] J. Kim, C. Ko, A. Frenzel, S. Ramanathan, and J. E. Hoffman, Appl. Phys. Lett. **96**, 213106 (2010).
[11] X. Zhong, X. Zhang, A. Gupta, and P. LeClair, J. Appl. Phys. **110**, 084516 (2011).
[12] A. Mansingh and R. Singh, J. Phys. C **13**, 5725 (1980).
[13] G. Stefanovich, A. Pergament, and D. Stefanovich, J. Phys. Condens. Matter **12**, 8837 (2000).
[14] N. Mott, Rev. Mod. Phys. **40**, 677 (1968).
[15] F. Morin, Phys. Rev. Lett. **3**, 34 (1959).
[16] A. Sharoni, J. G. Ramírez, and I. K. Schuller, Phys. Rev. Lett. **101**, 026404 (2008).
[17] H. T. Kim, B. G. Chae, D. H. Youn, G. Kim, K. Y. Kang, S. J. Lee, K. Kim, and Y. S. Lim, Appl. Phys. Lett. **86**, 242101 (2005).
[18] The physical mechanisms involved in the attachment of the particle to the tip end and its release on a surface

involve electrostatic interactions. These phenomena are complex and not fully understood and will be described in a future communication.

[19] L. Aigouy, G. Tessier, M. Mortier, and B. Charlot, Appl. Phys. Lett. **87**, 184105 (2005).

[20] F. Vetrone, R. Naccache, A. Zamarrón, A. J. de la Fuente, F. Sanz-Rodríguez, L. M. Maestro, E. M. Rodriguez, D. Jaque, J. G. Solé, and J. Capobianco, ACS Nano **4**, 3254 (2010).

[21] M. Alencar, G. S. Maciel, C. B. de Araujo, and A. Patra, Appl. Phys. Lett. **84**, 4753 (2004).

[22] Y. F. Chen, M. Ziese, and P. Esquinazi, Appl. Phys. Lett. **89**, 082501 (2006).

[23] A. S. Alexandrov, A. M. Bratkovsky, B. Bridle, S. E. Savelev, D. B. Strukov, and R. S. Williams, Appl. Phys. Lett. **99**, 202104 (2011).

[24] K. Okimura, N. Ezreena, Y. Sasakawa, and J. Sakai, Jpn. J. Appl. Phys. **48**, 065003 (2009).

[25] Complementary data with the particle placed exactly on the conducting path were not achieved due to the conducting path's small width and its appearance at random locations during various runs.